

## 45. ANALYSIS OF FULL WAVEFORM ACOUSTIC LOGGING DATA AT ODP SITE 642—OUTER VØRING PLATEAU<sup>1</sup>

Colleen Barton, Daniel Moos, and Jean-Pierre Blangy<sup>2</sup>

### ABSTRACT

Formation compressional and shear-wave velocities were calculated from sonic full waveform logs in ODP Hole 642E. The data were recorded over a 710-m interval of a cyclic repetition of lava flows and volcanoclastic sediments which are intruded by tholeiitic dikes. Although compressional ( $p$ ) and shear ( $s$ ) velocities in the flows are above 5 km/s and 3 km/s, respectively, interval velocities are 4.14 km/s for  $p$  and 2.25 km/s for  $s$ , resulting in an average  $V_p/V_s$  of 1.84 for the entire logged interval. This is a consequence of the much lower velocities in the volcanoclastics. The velocity results are interpreted in conjunction with the companion logs (density, porosity, natural gamma, and electrical resistivity) run in the drill hole in an attempt to determine the mechanisms causing the characteristic velocity response. The results show that porosity and microstructure have the primary influence on velocities. The degree of alteration to clay minerals is a secondary effect that requires the existence of initial pore connectivity.

### INTRODUCTION

Seismic investigations of the outer Vøring Plateau prior to Leg 104 of the Ocean Drilling Program were limited to marine refraction and reflection profiling summarized by Eldholm, Thiede, Taylor, et al. (1987), chapter 1. Site 642 was selected to investigate the evolution of the outer Vøring Plateau, specifically the wedge of seaward-dipping reflectors that are a part of the Vøring marginal high. The objectives of this investigation were to examine the events that occurred during the late rifting and early seafloor spreading evolutionary stage of a passive continental margin.

ODP Hole 642E cored over 900 m of material beneath about 320 m of sediment cover on the landward side of the Vøring Plateau escarpment. The basement lithologic units encountered in this drill hole are an upper and lower volcanic series differentiated on the basis of structure, texture, mineralogy, and geochemistry (Eldholm, Thiede, Taylor, et al., 1987). Both the upper series [337 to 1086.5 meters below sea floor (mbsf)] and the lower series (1088.5 to 1229.4 mbsf) consist of cyclic repetitions of volcanoclastic sediments and basalt flows. The upper and lower series are distinguished by the nature of the volcanoclastic sediments and basalts. Throughout the drilled section the basalts are usually brecciated at the tops of the flow sequences.

The logs collected in Hole 642E transected only the upper series volcanics. Within the upper series the volcanoclastics have a hypocrySTALLINE, tachylitic or aphanitic groundmass with clasts of highly vesicular tuffaceous internal fabric. Clay minerals include illite and kaolinite replacing pumice in vitric shards, and smectite and Fe-hydroxide alteration of clast fragments. The flows are fine- or medium- to fine-grained vesicular, aphyric basalt. The upper series has been subdivided into three groups based on grain size and degree of alteration.

### STANDARD LOGS

During Leg 104 a complete suite of standard Schlumberger logs was recorded in Hole 642E. These included caliper, natural gamma, spectral natural gamma (from which K, U, and Th concentrations can be determined), induction resistivity, neutron

porosity, gamma-gamma density, and sonic traveltime (picked during logging). All of the standard log measurements were good except for the caliper log. The lack of variability in the caliper data indicates that the caliper arm was not functioning properly. Therefore the caliper data were not used in this analysis. Results of the compensated neutron log, which is sensitive to lithology (see Lysne, this volume and the discussion below) were inconsistent with porosity values determined from core measurements and computed from the density log.

Figure 1 gives the extent of the logged interval for each logging tool run in Hole 642E and the simplified sketch of the lithologic column as defined by petrographic analysis of the core. The sonic logging data recorded in the dipping reflector sequence during Leg 104 represent the first *in-situ* velocity measurements available for the outer Vøring Plateau. The data can be used to determine the detailed seismic character of the basement rocks, for correlation with seismic refraction data, and as time ties for seismic reflection data. Core recovery was approximately 40% over the basement interval drilled in Hole 642E and the sonic data, when correlated with the other geophysical logs, provides well-constrained depths for lithologic horizons. (See Shipboard Scientific Party, 1987.)

The sonic velocities recorded during ODP Leg 104 also provide new information about the character of the basement rocks of the outer Vøring Plateau. As elastic properties are a complex function of mineralogy, alteration, and microstructure, we interpret the sonic data in conjunction with the companion logs run in Hole 642E to determine the parameters controlling the seismic character of the rocks and to discriminate between primary lithologic and secondary structural effects. The logs are unusually high quality for ODP data, and abundant core information is available. The results of this log analysis may be used as a guide at similar oceanic sites with either poorer core recovery or lower quality log data.

### SONIC WAVEFORMS

Conventional sonic logging tools are designed with one or two sources and a pair of receivers where only the delay time of the compressional headwave is recorded. Full-waveform acoustic logging tools generate a complete microseismogram, typically with four or more source receiver combinations at longer source receiver separation than conventional sonic tools. They record the arrival time of both body and surface waves propagating through the borehole fluid and the surrounding forma-

<sup>1</sup> Eldholm, O., Thiede, J., Taylor, E., et al., 1989. *Proc. ODP, Sci. Results*, 104: College Station, TX (Ocean Drilling Program).

<sup>2</sup> Dept. of Geophysics, Stanford University, Stanford, CA 94305.

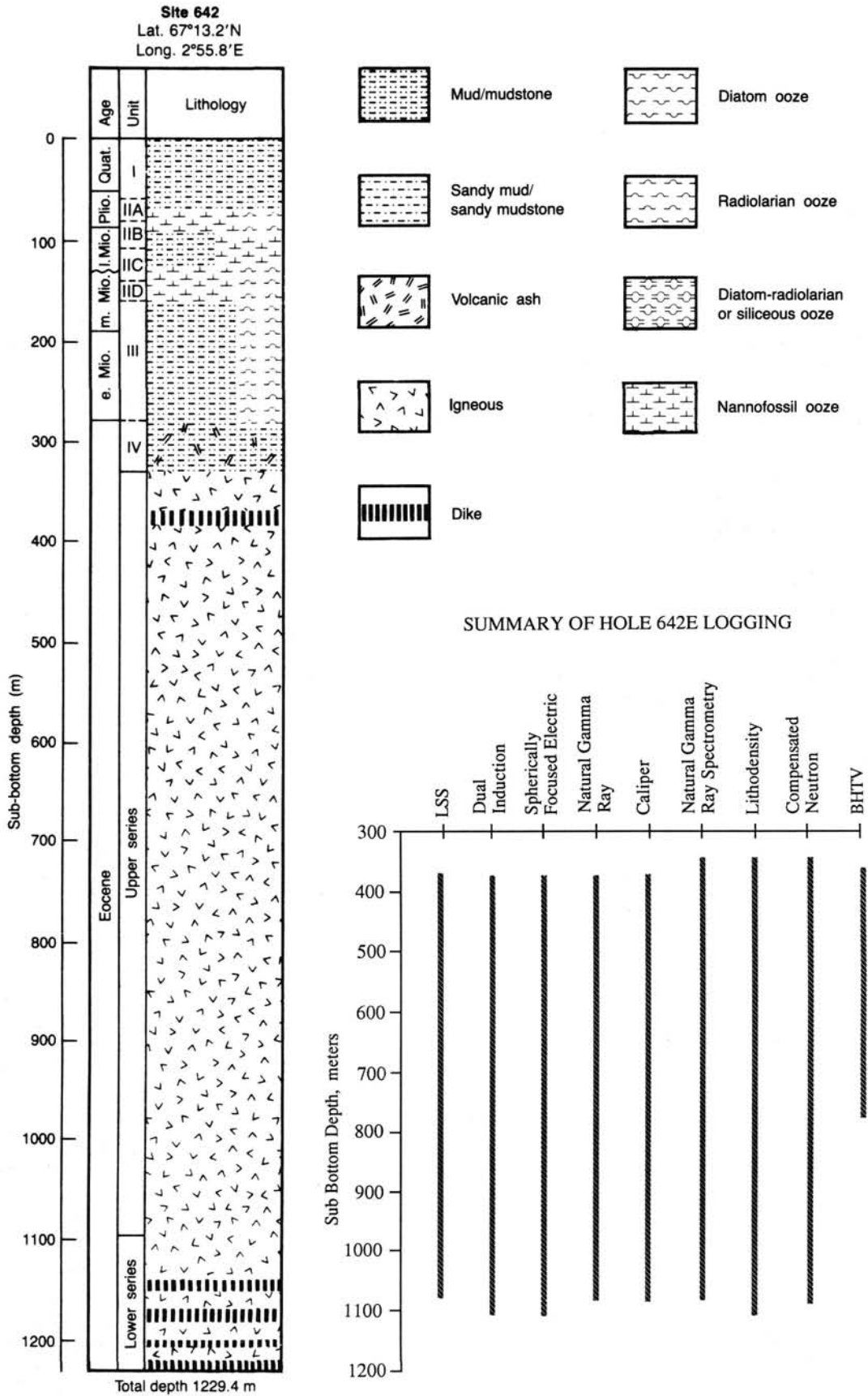


Figure 1. Summary of logging completed in Hole 642E during ODP Leg 104 compared to the lithologic column.

tion. Two groups of elastic waves propagate in a borehole: head waves, the compressional and shear modes, and the borehole-guided waves, generally the normal modes or pseudo-Rayleigh waves and Stoneley waves. The compressional wave propagates through the borehole fluid, is critically refracted in the formation, and then refracted back into the fluid as a compressional wave. The shear wave begins as a compressional wave in the fluid, is converted to a shear wave in the formation, then refracted back into the fluid as a compressional wave. Shear and compressional waves are sensitive to the effective elastic moduli of the formation. The guided waves are borehole surface waves, they are dispersive, and arrive after the onset of the shear wave. These waves are affected by the formation parameters as well as the borehole surface. The guided waves generally have higher amplitudes and longer durations than either the compressional or shear waves.

Wave propagation in cylindrical boreholes is extremely complex due to the presence of head waves, trapped fluid modes, and surface waves. Determining which modes are recorded after the onset of the compressional arrival is therefore difficult. For typical logging geometries with the LSS sonde deployed in Hole 642E, pseudo-Rayleigh waves will be strongly excited. At relatively short source-to-receiver spacings this phase could be confused with a direct shear arrival (Paillet and White, 1982). Further, synthetic acoustic logs indicate that the shear-wave arrival cannot be distinguished from the first cycle of the pseudo-Rayleigh wave (Cheng and Toksöz, 1980, 1981; Tsang and Rader, 1979). Because the pseudo-Rayleigh velocity at the cutoff frequency is equal to the shear velocity of the formation, the measurement of either the shear arrival or the onset of the pseudo-Rayleigh wave is a measurement of the shear velocity of the formation (Willis and Toksöz 1983), provided that energy at the cutoff frequency is present in the recorded wavetrain.

We used the compressional wave delay time and the formation density from the logs along with borehole size information estimated from the size of the 10.36-cm drill bit to evaluate the frequency content of the shear waves present in the data recorded during Leg 104. Synthetic dispersion curves were computed using a range of velocities and densities to model those expected in Hole 642E (modeling after Cheng and Toksöz, 1981). Figure 2 shows the cutoff frequencies for the pseudo-Rayleigh waves expected in this data, along with the model parameters used to compute the dispersion curves. The cutoff at about 8.9 kHz suggests that low-pass filtering of the data at 10 kHz would remove any ambiguity from analysis of the shear wave by the semblance technique. A low-pass 10-kHz Butterworth filter was used to process the data before the semblance analysis was performed, and it was determined that the bandwidth of the LSS tool was sufficient to record shear arrivals over most of the logged interval. The exceptions, of course, are the intervals where the shear velocity is lower than the borehole fluid velocity. These occur within the volcanoclastic layers at several depths (cf. 720 and 747 mbsf).

Seven hundred and fifteen meters of interbedded basalt flows and volcanoclastic sediments transected by Hole 642E were logged with the standard four-channel Schlumberger LSS tool. The tool is configured with two sources and two receivers having separations of 2.44, 3.05, 3.05, and 3.66 m. The recording frequency range is from 10 to 20 kHz and the sampling interval was 5  $\mu$ s. The waveforms generated in Hole 642E were recorded for a total time of 2.56 ms. Data include waveforms from each source-receiver pair.

Figure 3 shows data from each of the four receivers, with the two 3.05-m spacings offset for clarity. Both filtered (right-hand panel) and unfiltered data are shown. The near-spaced receiver pair recorded data of better quality than that recorded by the far-spaced receiver pair and thus the near-spaced pair was used exclusively for the velocity analysis.

The sonic waveforms recorded in Hole 642E provide a distinct characterization of the different lithologic units. Waveforms recorded in the fine-grained massive basalt units at 831 mbsf (Fig. 3A) generally have strong compressional energy (0.43 ms for the near receiver) and shear energy (0.88 ms for the near receiver). Normal modes arrive shortly after the shear wave and are not directly identifiable. Filtering removes the high-frequency normal modes following the shear wave, but shear and compressional arrivals are still quite distinct. Figure 3B, from 581 mbsf, shows a typical waveform recorded in volcanoclastic sediments. Both the compressional (0.66 ms) and shear/pseudo-Rayleigh (1.5 ms) amplitudes are significantly reduced in this lithology. Filtering removes all of the identifiable energy within the shear window. In a typical brecciated zone at 910 mbsf (Fig. 3C), the compressional (0.6 ms) and shear/pseudo-Rayleigh (1.6 ms) amplitudes are again reduced with respect to waveforms recorded in the massive units. The strong arrival at 1.6 ms is almost entirely eliminated by filtering, suggesting that most of its energy is significantly above the pseudo-Rayleigh, low-frequency cutoff (see Fig. 2). Thus filtering has in each case eliminated spurious energy within the shear window, as desired, leaving only the true shear wave.

The compressional wave arrival can be traced easily in waveform plots of the unfiltered data at the near receiver (Fig. 4). The shear pseudo-Rayleigh arrival is less easily distinguished. Both arrivals are extremely variable over narrow depth ranges. At 580 mbsf, where there is a 2-m layer of tuffaceous sediments, the guided waves essentially disappear, reflecting their sensitivity to the formation shear velocity. Within this same interval compressional and shear arrivals are delayed and have sharply lower amplitudes.

## VELOCITY DETERMINATION

In this study compressional and shear-wave velocities were measured through a semblance correlation technique (Kimball and Marzetta, 1984; Moos et al., 1986; Goldberg et al., 1986; Moos, 1988). Semblance is a measure of the correlation between arrivals and is calculated as the ratio of the sum of the  $k$ th lag time-shifted cross-correlations of the windowed data at  $M$  receivers divided by the zero lag autocorrelation within each window:

$$S_C(K) = \frac{\sum_{J=K-N/2}^{K+N/2} \left[ \sum_{I=1}^M f_{IJ} \right]^2}{\frac{1}{M} \sum_{J=K-N/2}^{K+N/2} \sum_{I=1}^M (f_{IJ})^2} \quad (1)$$

Here  $N$  is the window width, chosen to be equal to the width of the expected duration of several cycles of the arrival, and  $M$  is the number of receivers. Semblance values can range between 0 for random coherence and 1 for perfect coherence between the windowed arrivals at each receiver. The highest semblance occurs when the window lag between the two waveforms is the product of the slowness and the offset. In this analysis the time window was fixed at the near receiver to reduce the computational time, as discussed below.

The semblance analysis technique permits the use of a narrow time window of data for each correlation, thereby reducing the possibility of interference between the different phases. Velocities within ODP Hole 642E have narrow depth ranges, which presents two difficulties in the data analysis. First, a constant adjustment of the start time of the semblance is required to ensure that the correct mode is within the correlation window. In

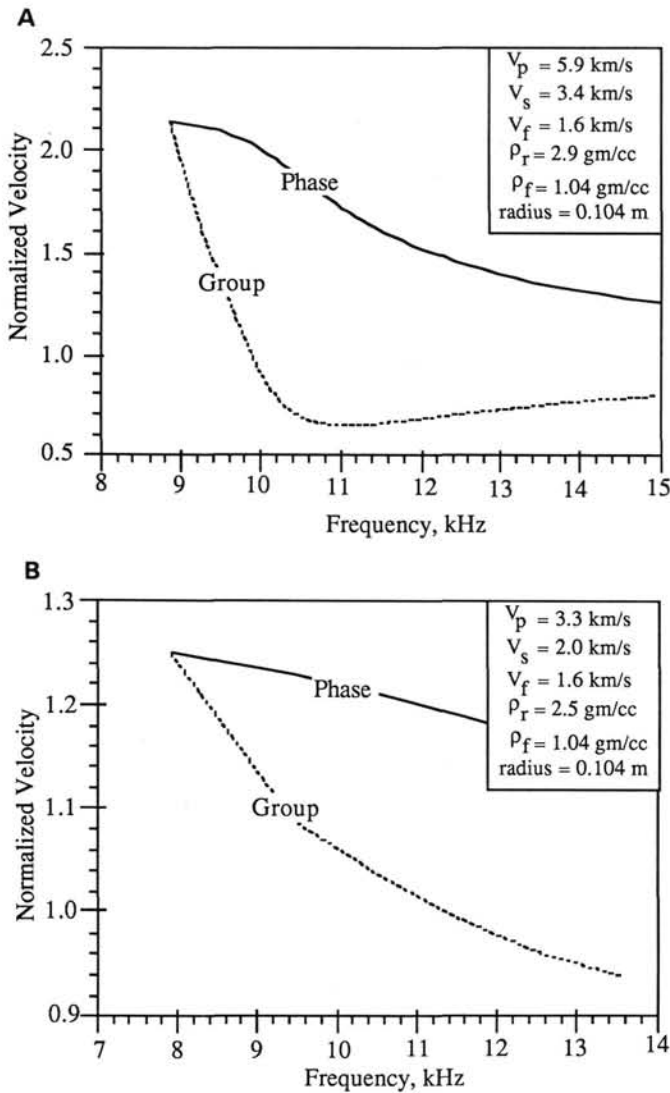


Figure 2. Dispersion curves calculated from model parameters listed in the insets. A. Intact basalt model parameters result in a cutoff frequency at about 9.4 kHz. B. Model using typical volcaniclastic formation parameters has a slightly lower cutoff frequency.

addition, the range of acceptable slowness values in these data cannot be well constrained, and calculation of nonunique semblance peaks within the acceptable range was not uncommon. To alleviate both of these difficulties in the standard semblance analysis, interactive graphics algorithms were developed to adjust start time with depth and, after semblance is calculated, to interactively determine the unique slowness value at peak semblance for each record.

A window of 200  $\mu$ s was used to compute the compressional arrival semblance with slowness constraints between 144 and 476  $\mu$ s/m (44 and 145  $\mu$ s/ft) corresponding to velocities between 2.1 and 6.9 km/s. The window used for the shear computation was 500  $\mu$ s long with slowness between 308 and 640  $\mu$ s/m (94 and 195  $\mu$ s/ft) corresponding to velocities between 1.6 and 3.2 km/s. The semblance correlation technique proved to be very successful for the compressional wave modes throughout the logged interval. The semblance results for the shear mode were good in the massive basalt layers, but were less reliable in the volcaniclastic intervals. It is likely that these high-porosity beds have formation shear velocities that are approximately equal to the fluid velocity, prohibiting the critical refraction of the shear

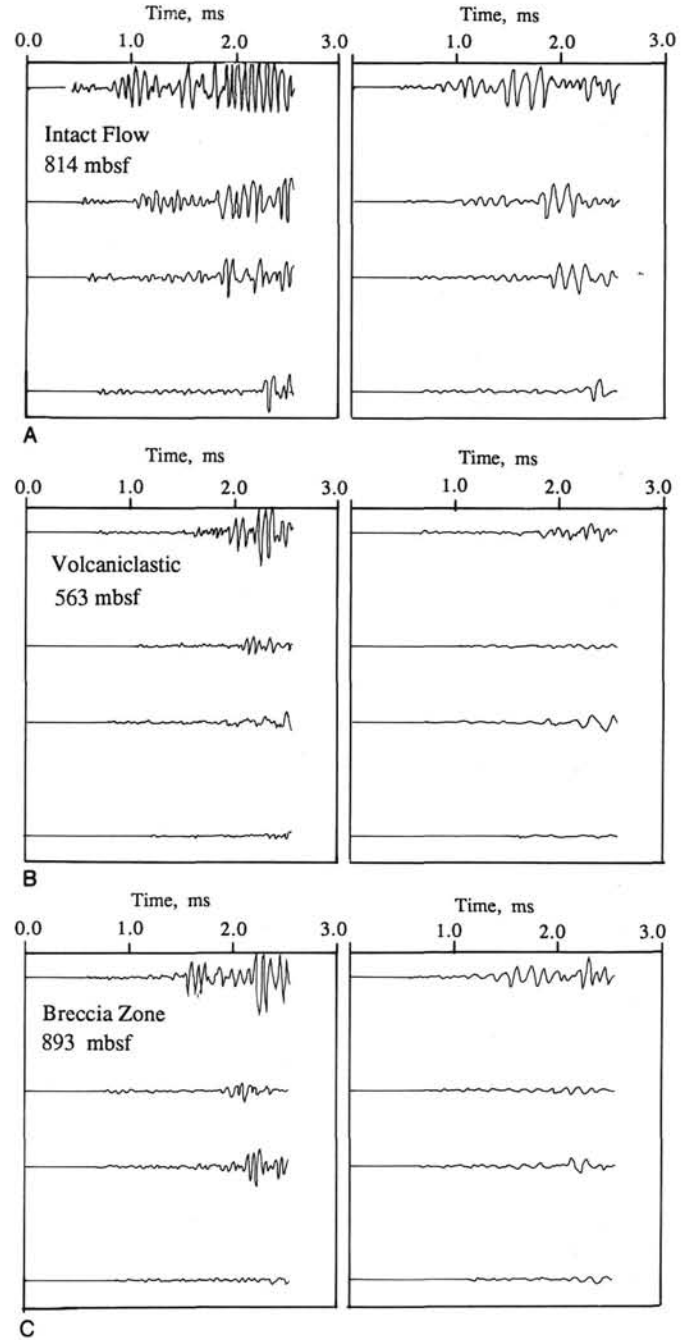


Figure 3. Sonic full waveform suites at selected depths. The left-hand panels show the raw waveforms, and the right-hand panels show the data after the application of a 10-kHz low-pass filter. Top: Waveforms recorded in fine-grained massive basalt at 814 mbsf with compressional arrival at 0.43 ms and shear/pseudo-Rayleigh arrival at 0.88 ms. Significant shear energy is present after filtering. Middle: Waveforms recorded at 563 mbsf representing volcaniclastic sediments, with compressional arrival at 0.66 ms and shear/pseudo-Rayleigh arrival at 1.5 ms. After filtering little shear energy remains. Bottom: Waveforms recorded in a typical brecciated zone at 893 mbsf with compressional arrival at 0.6 ms and the shear/pseudo-Rayleigh arrival at 1.2 ms. Gains are adjusted to allow data comparisons. Again filtering removes most of the pseudo-Rayleigh energy, leaving little refracted shear wave in the data.

wave. Furthermore, energy within the shear window is contaminated by other borehole modes.

The results of the velocity analysis for the data from Hole 642E are given in Figure 5. Compressional and shear velocities

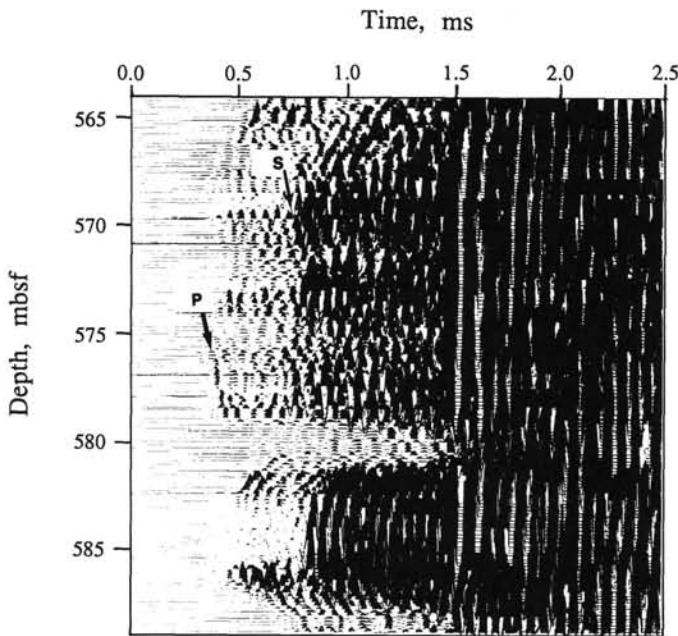


Figure 4. Waveform plot of one of the 2.44-m receivers. The compressional arrival,  $V_p$ , is easily traced but the shear arrival is more difficult to distinguish. Both compressional and shear arrivals are extremely variable over narrow depth ranges.

are plotted with depth along with the ratio  $V_p/V_s$ . The slowness values were averaged over 0.5 m for each profile. Compressional velocities range between 3.51 km/s and 5.93 km/s within the basalt flows and between 2.82 km/s and 3.35 km/s in the interlayered volcanoclastic sediments. There is a distinct cyclic behavior of the velocities that shows excellent correlation with the lithologies determined by petrographic analysis. Compressional velocities appear to be more variable than shear velocities which fluctuate between 2.04 km/s and 3.25 km/s in the basalts and 1.83 km/s and 3.22 km/s in the volcanoclastic sediments. Overall trends in compressional and shear velocities with depth are not observed. The  $V_p/V_s$  ratio is approximately 1.9 throughout most of the interval. The ratio is 30% higher in the competent basalts than in the volcanoclastics. Extreme high and low values at the boundaries between flows and volcanoclastics are due to slight differences in the critical angle of refraction for shear and compressional waves. These mismatched boundaries are errors to be ignored in the data interpretation.

The mean semblance (the product between shear and compressional semblance) is highest in the competent basalts and lowest in the low-velocity volcanoclastic layers. This is due primarily to the heterogeneities in the volcanoclastics, compared to the more homogeneous flows. Semblance increases somewhat below 586 mbsf, reflecting an increase in waveform coherence.

#### ANALYSIS OF STANDARD LOGS

Preliminary analyses of the log measurements are given in Eldholm, Thiede, Taylor, et al. (1987). Our purpose in presenting the logs here is to integrate the full waveform analysis with the additional information from the standard logs. Log data typically need some corrections before the measurements can be interpreted. Some measurements, such as sonic compressional velocity or formation resistivity, are direct. Others, such as gamma-gamma density or neutron porosity, are inferred from the transport properties of the formation for gamma-rays or neutrons, and rely on empirical relationships and assumptions about the chemistry of the formation components (e.g., Serra, 1984). Log responses are calibrated within sedimentary rocks;

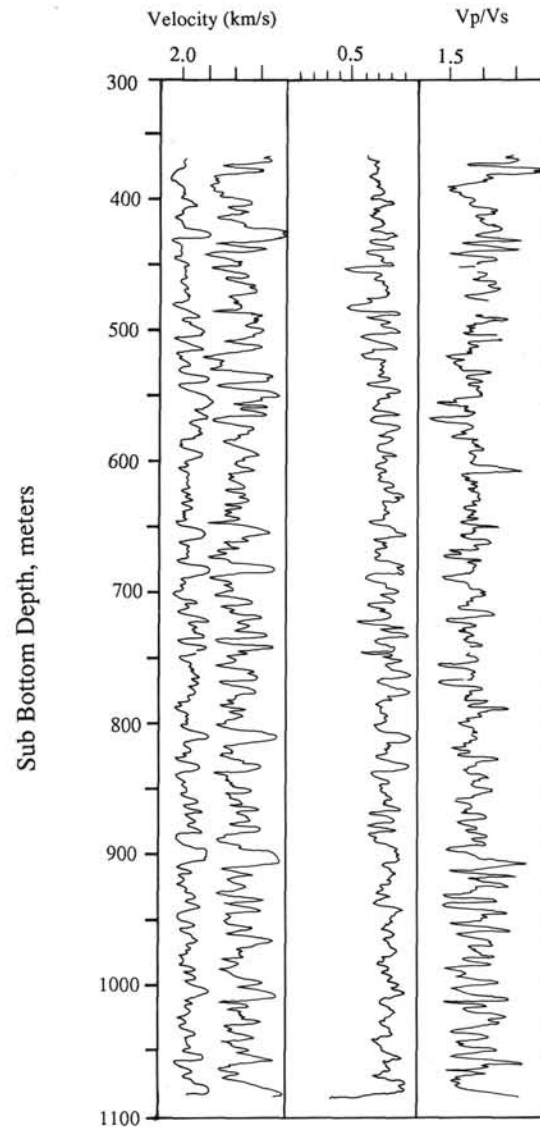


Figure 5. Results of the semblance analysis in ODP Hole 642E. Track 1, curve 1, is measured shear velocity; track 1, curve 2, is measured compressional velocity. Track 2 shows the geometric mean of the shear and compressional semblances. Track 3 is the ratio  $V_p/V_s$ .

generally the response in basaltic rock is assumed to be adequately described using the calibrations for limestone lithologies. However, large errors can be introduced if geochemistry and alteration state are not considered (Lysne, this volume).

In this analysis we follow the general principles outlined in Broglia and Moos (1988). They presented a careful analysis of logs recorded during ODP Leg 102 in the 110-Ma basaltic crust of Layer 2 in DSDP Hole 418A. To avoid needless repetition we will simply present the steps taken to reduce the raw data prior to display, and avoid rediscussing in detail the justifications.

In general one assumes that shipboard physical properties accurately represent the recovered material. Therefore, in unfractured intervals of 100% core recovery, log and core measurements should match. We choose for our comparison a flow unit designated F84 in the interval between 890 and 920 mbsf (Fig. 6). Within this interval (Cores 104-642E-73 and -74) core recovery was greater than 90%. Shipboard physical properties recorded during ODP Leg 104 included bulk density and ultra-

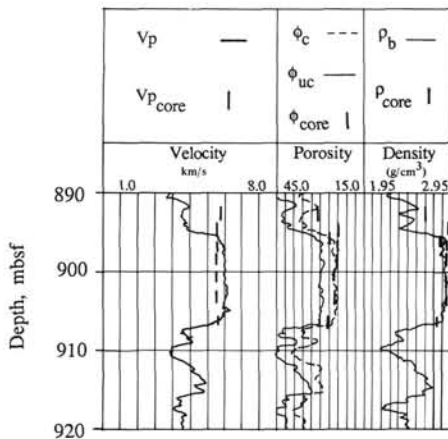


Figure 6. The relationship between the raw log curves and the core data (vertical bars) within the interval 890 and 910 mbsf. Densities are almost identical. Velocities from the logs are slightly lower than those measured from core. Log porosities are about 7 to 11 porosity units too high; the corrected curve is obtained by subtracting 8 porosity units.

sonic compressional velocity recorded along the core and in two orthogonal directions across each sample (Eldholm, Thiede, Taylor, et al., 1987). No porosity determinations were made, which is extremely unfortunate because of the anomalously high thermal neutron absorption in these rocks. Lysne (this volume) estimates that raw neutron porosities are 8 to 10 porosity units too large. Grain density can often be computed from normative mineralogy, but the data are insufficient in these samples to attempt this calculation. We therefore computed effective core porosities assuming a grain density within the selected interval of  $2.98 \text{ g/cm}^3$  and the relationship:

$$\phi = \frac{\rho_g - \rho_b}{\rho_g - \rho_f} \quad (2)$$

Core and logged densities are almost identical (Fig. 6, track 3). Velocities from the logs are slightly lower than velocities measured in the core (Fig. 6, track 1), due perhaps to the presence of several mineralized fractures within this interval that slightly reduce the *in-situ* velocities (e.g., Moos and Zoback, 1983; Stesky, 1986). Log porosities are about 7 to 11 porosity units too high (Fig. 6, track 2) in agreement with Lysne (this volume) predictions and with similar results found by Broglia and Moos (in press). We therefore apply no correction to the density curves, and subtract 8 PU from the neutron curves, to obtain lithology-corrected log responses within Hole 642E. Note that this correction will be reasonable provided the concentration of neutron absorbers is relatively constant. No corrections were applied to the natural gamma logs or resistivity measurements. The single largest factor affecting these logs is hole size (Schlumberger, 1974). Unfortunately, due to the poor quality caliper data it is difficult to determine the location of washouts (hole enlargements) that degrade density and porosity logs which rely on good contact between the source-detector skid and the borehole wall.

As the neutron log responds primarily to the presence of hydrogen (regardless of whether it is associated with pore fluids or is bound within hydroxides), the neutron log must be further corrected for clay content. The clay components include low-temperature smectite alteration products and kaolinite and illites (Eldholm, Thiede, Taylor, et al., 1987) and are primarily concentrated within sedimentary units between the primary flows. Following the technique of Broglia and Moos (1988), we estimate the clay volume from the K curve provided by the natural

gamma spectrometry log. We were unable to determine the relationship between the log value of K in weight percent and clay volume directly, because no estimates of clay volume were available. Therefore, we assumed a normative potassium content for an average clay of 8 percent by weight (Deer, Howie, and Zussman, 1966) and a "clay porosity" of 44% to obtain the relationship:

$$V_{cl} = \frac{K \text{ (wt\%)} (\rho_b/\rho_{cl})}{0.08} \quad (3)$$

and therefore

$$\phi_c = \phi_n - 44 V_{cl} \quad (4)$$

The density ratio in equation (3) is necessary to convert from weight percent to volume percent. Note that this correction does not take into account the Fe hydroxide associated with clay alteration in these rocks. Further, it assumes a constant stoichiometric ratio of K to H in the clays.

The final log results are shown in Figure 7 as a function of depth. Included are natural gamma in API units,  $V_{cl}$  in volume percent, deep-induction (ILD) and spherically focused laterolog (SFLU) resistivities in ohm-m plotted on a logarithmic scale, density (RHOB) in  $\text{g/cm}^3$ , corrected porosity (NPHIF) in percent, and compressional sonic velocity (VEL) in km/s. Shading is applied between 0 and the clay content to emphasize the results. Density and porosity are plotted so that the two curves will overlies if grain density is  $3.00 \text{ g/cm}^3$ , and shading is applied between the two whenever density is less than expected for a given porosity. Shading is also applied whenever the SFL resistivity is greater than ILD resistivity.

Variations in physical properties are generally as expected for these rocks. The volcanoclastics between flows have generally low velocities, densities, and resistivities, and high porosities, natural gamma activity, and clay content. In shallower sections density reads sharply lower than expected within volcanoclastics characterized by high gamma-ray values (e.g., 371–381, 399–405, 447, and 451 mbsf). Deeper in the hole this effect is less pronounced, suggesting that it is due in part to poor density pad contact within washouts in the less competent sediments. This supposition is supported by the erroneous velocity determinations within the same zones, especially at 447 and 451 mbsf. The density log has not been corrected for clay, and thus some of this effect may be due to the lower clay density. In addition, the higher water content within these intervals causes anomalously low density readings. Overcorrection of the neutron for clay may also contribute to this difference. Within the flows, densities, velocities, and resistivities are high, and porosity and clay content are low. The total gamma activity does not precisely track clay, as U and (primarily) Th also contribute to the total. Interestingly, this difference is larger within the flows, suggesting a higher concentration of U and/or Th.

Resistivity is a particularly sensitive indicator of porosity, and the relationship between resistivity and neutron porosity in clay-free zones has been intensely studied (e.g., Brace et al., 1965; Archie, 1942). This relationship is of particular interest within Hole 642E, where resistivities above about 100 ohm-m uniquely characterize the flows. Unfortunately, induction logs typically saturate when formation resistivities are more than three orders of magnitude greater than borehole fluid resistivities. The resistivity of the borehole fluids (fundamentally identical to that of seawater) can be expressed as:

$$R_w = (3 + T(^{\circ}\text{C})/10)^{-1} \quad (5)$$

(Von Herzen et al., 1983). For a sediment geothermal gradient of  $0.08 \text{ }^{\circ}\text{C/m}$  inferred from sediment resistivities recorded in

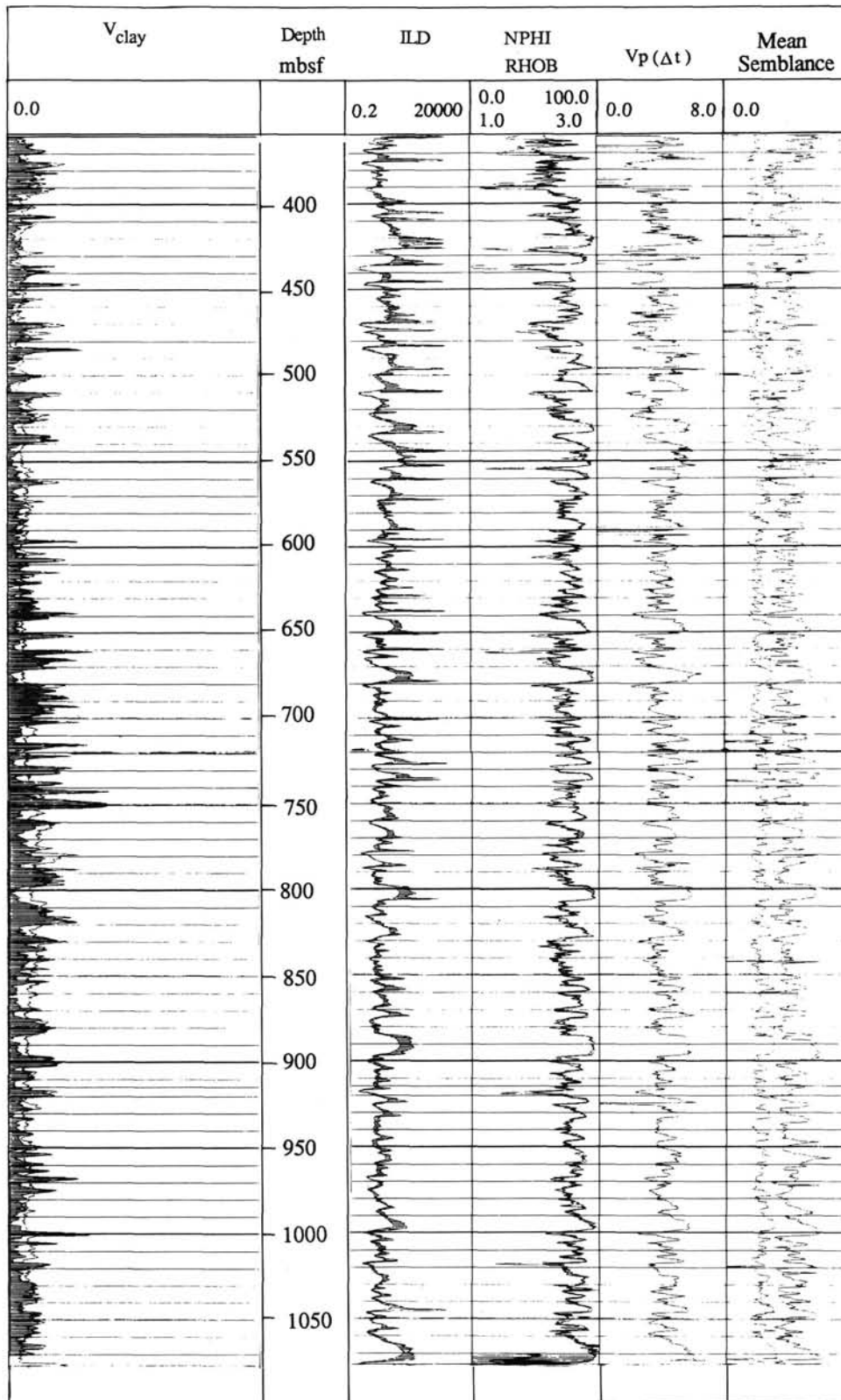


Figure 7. The corrected logs for ODP Hole 642E over the interval 369 to 1098 mbsf. Included are the natural gamma in API units,  $V_{cl}$  (clay volume) in volume percent, deep induction (ILD) and spherically focused laterolog (SFLU) resistivities in ohm-m plotted on a logarithmic scale, density (RHOB) in  $gm/cm^3$ , corrected porosity (NPHIF) in percent, and compressional sonic velocity (VEL) in km/s. Shading is applied between 0 and the clay content to emphasize the results.

Hole 642D and index thermal properties (Eldholm, Thiede, Taylor et al., 1987) and from the assumption that the geothermal gradient within the flow sequence is about half that of the sediments [based on typical ratios of sediment to basalt thermal conductivities (e.g., Becker, 1985), temperatures range from 30°C at the top of the logged section (371 mbsf) to 60°C at the bottom of the logged section (521 mbsf)]. Using these temperature values the fluid resistivity varies between 0.17 and 0.11 ohm-m. Thus the ILD reads too low whenever formation resistivity is greater than 100 to 200 ohm-m. This effect can clearly be seen in the data, where ILD reads as much as 200 ohm-m less than SFLU within the flows. Thus SFLU is a more reliable measure of formation resistivity.

At the base of many of the flow units SFLU reads more than 2000 ohm-m. Ordinarily one would expect the other porosity-sensitive logs to respond similarly and in some instances high velocities and densities and low porosities accompany the high resistivities (e.g., at 1810 mbsf). In general, however, the other logs do not detect these zones, suggesting that they are less than 0.5 m thick—near the resolution of volume-averaging devices such as density or porosity. If the resistivity change is due to changes in pore connectivity without changing the pore volume, none of the other logs will detect the change. In this case changes in the ratio  $V_p/V_s$  would be expected within these zones.

Cross-plots of the different log measurements emphasize the relationships between logged physical properties. Figure 8A shows the relationships between density and porosity for the entire well, including flows, breccias, and volcanics. Figure 8B is a cross-plot of density and porosity excluding zones with high (>5%) clay. This isolates primarily the flows and breccias and excludes the volcanics. A strong linear trend is revealed in both plots, matching the theoretical relationship between bulk density and porosity for a grain density of 3.00 g/cm<sup>3</sup>. The volcanics plot below the line, as expected, due to anomalously low measured bulk density (see also Fig. 7). The linear relationship implies that mineralogy is relatively constant within the clay-poor zones, and that changes in physical properties must therefore be due largely to other effects.

Figure 9A is a cross-plot of velocity vs. porosity for the entire logged interval. Velocity generally decreases with porosity, as expected, but scatter in the data makes it difficult to determine whether a time-average

$$1/V = \phi/V_w + (1 - \phi)/V_g \quad (6)$$

or volume-average

$$V = \phi V_w + (1 - \phi)/V_g \quad (7)$$

is a better fit to the data. The relationship between bulk density and sonic velocity illustrated in Figure 9B is a consequence of the relationships between density and porosity, and porosity and velocity, discussed above.

The cross-plots above demonstrate that the standard log data are of consistently high quality. Furthermore, the single trend in the data (once the clay-rich zones have been excluded) indicates that the only major change in this well is structural, confirming the results of shipboard core analyses (Eldholm, Thiede, Taylor et al., 1987) that primary mineralogy is relatively constant. Thus variations in the elastic properties are primarily due to structure.

## VELOCITY EFFECTS FROM MICROSTRUCTURE

The elastic properties of the volcanics and of the basalt flows are quite different, in spite of their compositional similarities. These differences are due to the larger porosity of the volcanics, as well as to differences in alteration. Both weathering (primary alteration) and replacement (secondary altera-

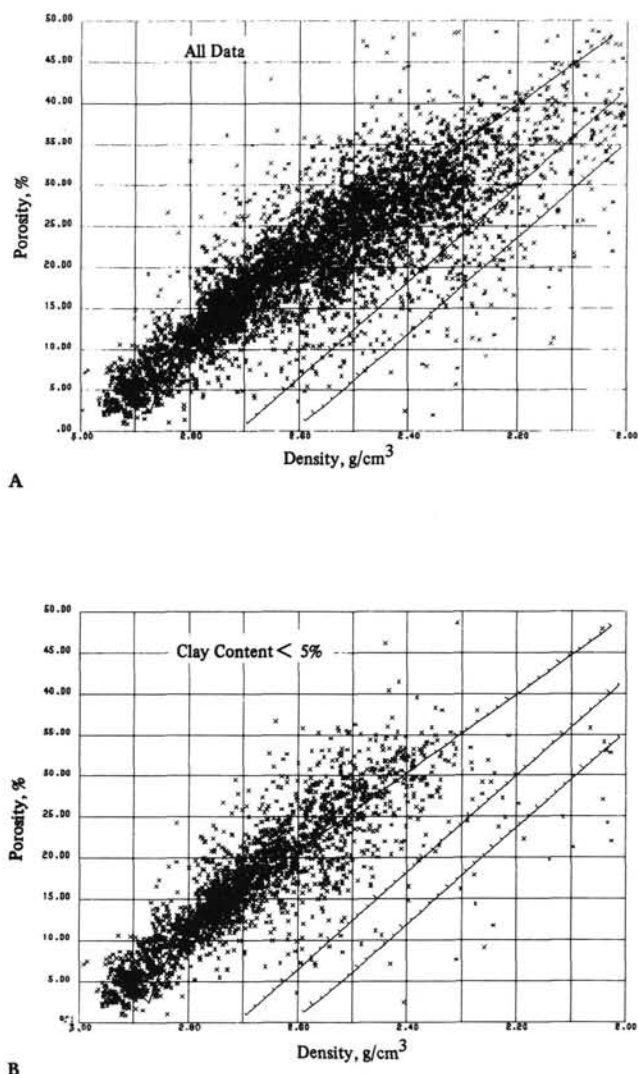


Figure 8. The effect of clay on the relationship between porosity and density: A. Porosity vs. density for the entire well; B. Porosity vs. density for units with clay content less than 5%.

tion) effects are present. The former acts to decrease the velocities by weakening the matrix material, and the latter increases the velocities by infilling pores and cracks. These effects may also result in subtle differences between the velocities within the flows themselves. If so, careful analysis of the velocities and clay content may provide clues to the emplacement and alteration history of the different units.

The effect of microstructure on elastic waves has been extensively studied in field and laboratory experimentation. Unfortunately, very little work has been published for the rock types drilled in Hole 642E. It is also well established that the presence of joints and fractures affects seismic velocities *in situ* (King et al., 1978; Stierman and Kovach 1979; Stephanson et al., 1979; Swolfs et al., 1981; Moos and Zoback, 1983). *In-situ* velocities are generally lower than those measured in laboratory samples from the same site. The differences correlate with fracture frequency and volume sampled; however, the correlation varies in different areas and for different rock types. Sonic velocities within the 10- to 20- kHz range are influenced by fine-scale microcracks, whereas seismic velocities in the 10- to 50-Hz frequency range are also affected by joints and fractures. In this study therefore, we are primarily concerned with the microcrack

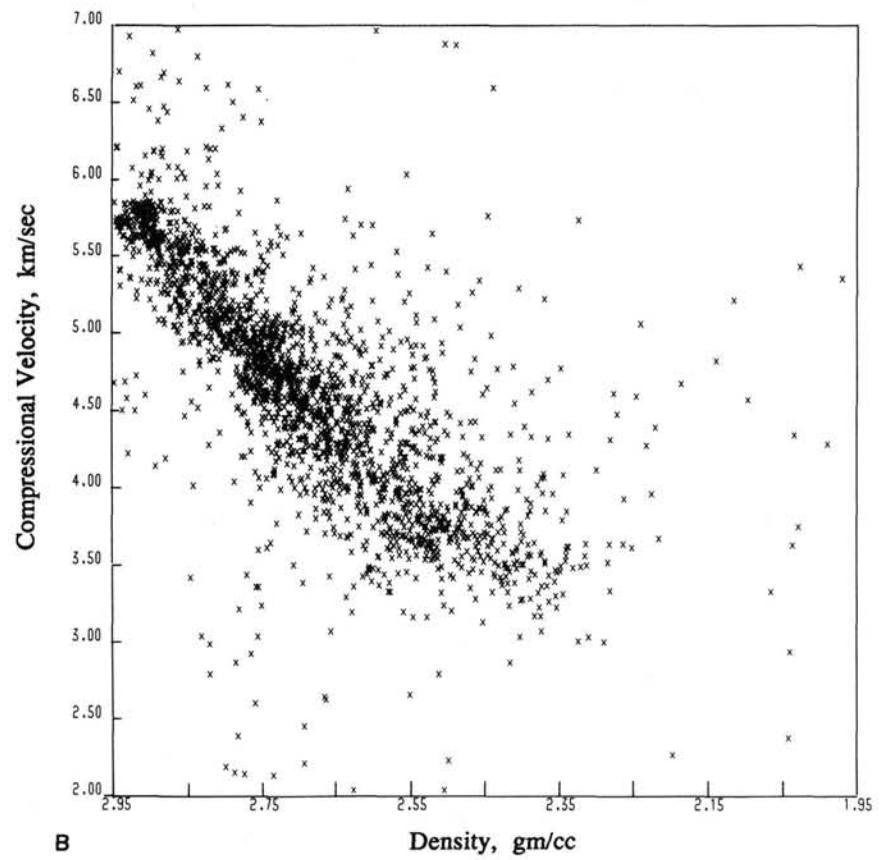
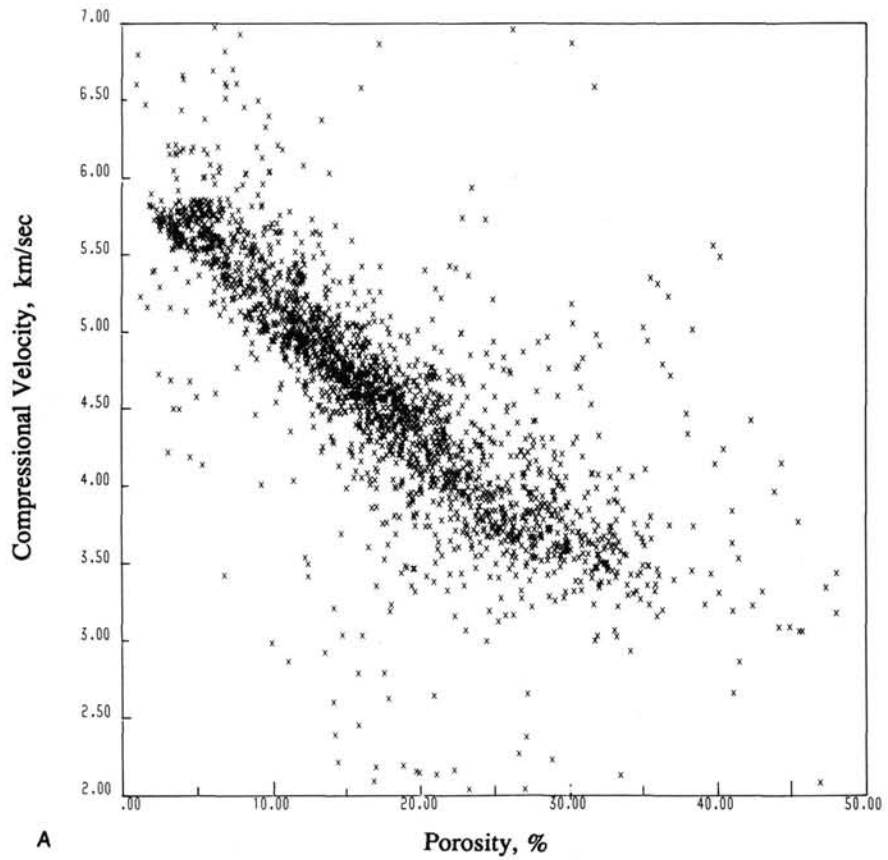


Figure 9. Cross plots of the primary log physical properties, for units with clay content less than 5%: A. Velocity vs. porosity; B. Velocity vs. density.

effects on velocity. Theoretical work on the influence of pore shape on velocities indicates that slender pores reduce stiffness and subsequently reduce both bulk and shear moduli (Timoshenko and Goodier, 1934). For round pore models in low-porosity media,  $1/K$  increases linearly with porosity. For pores with lower aspect ratio,  $1/K$  is proportional to crack length cubed (Nur, 1980).

The interrelation of fractures and weathering (primary alteration) was seen to be the controlling influence on sonic compressional and shear velocities, in a study of crystalline rocks by Moos and Zoback (1983). Velocity variations could not adequately be explained by a model of a dense concentration of microcracks but rather by the subsequent alteration by fluid flow through the microcracks.

Laboratory work by Turuta et al. (1967) shows an extreme decrease in compressional velocities with increasing interfaces. Stesky (1986) conducted experiments on 15 igneous and metamorphic rocks by making successive sawcuts to rock samples and measuring compressional and shear velocities with increasing confining pressure. The presence of the sawcuts lowered both compressional and shear velocities. The velocities of low crack-porosity rocks are most markedly affected by the addition of cuts, whereas high crack-porosity rocks show relatively less decrease in velocity. The change in compressional velocity at low confining pressure (5 MPa) for the low crack-porosity rocks (metabasalts) from 0 to 4 sawcuts was 58% and shear velocity decreased 31%. For rocks with higher crack-porosity (porphyritic granite) compressional velocities decreased 12% and shear velocities decreased 31%.

To examine the relationship between microstructure and velocity in detail, the velocities measured within the interval 711 to 761 mbsf are shown in Figure 10 correlated with the corresponding section of the lithostratigraphic column determined from petrographic analysis. This interval corresponds to a series of seven fine-grained upper series flows petrographically classified as Group II. Three of the flows show a slight decrease in  $V_p/V_s$  ratio; the remaining flows have an increasing  $V_p/V_s$  ratio with depth. These trends are observed over the entire logged interval.  $V_p/V_s$  is generally lower in the volcanoclastic zones. Note that at interfaces the boundary observed in  $V_p$  is often slightly deeper than the boundary detected in  $V_s$ . This is due to the slight offset in the interval over which the two head waves arrive as they propagate through the formation. This difference gives rise to the erroneous peaks in  $V_p/V_s$  at these sharp boundaries.

Compressional- and shear-wave velocities within the interval 861 to 911 mbsf are shown in detail in Figure 11. At this depth there is a transition from the petrographically defined Group II to Group III flow types. The flow interval 872 to 879 mbsf and 896 to 910 mbsf represent a flow type that does not show a gradual increase in velocity with depth. This contrasting flow type is commonly nested between a series of flows that do show a velocity gradient. It is clear from the lithologic sections that these constant-velocity sections have less alteration than the flows with velocity gradients.

Figures 10 and 11 also show the corresponding  $V_{cl}$  curve over these 50 m intervals. From this comparison it is clear that clay content is not the only factor controlling the velocities over these intervals. To determine the magnitude of the effects of primary alteration it is illustrative to consider the  $V_{cl}$  curve along with the velocities through crossplots of  $V_p/V_s$  vs. clay content. Two primary types of flows are found, characterized by (a) sharply increasing  $V_p$  with depth (Fig. 12A1, A2) or (b) constant  $V_p$  (Fig. 12B). Type (a) has decreasing  $V_p/V_s$ . Type (a) sometimes has decreasing clay (Fig. 12A1); in other cases clay content is uniformly low (Fig. 12A2). The examples of these three types plotted in Figure 12 are interpreted as follows: (A1), 720 to 726 mbsf, with velocity ratio 1.6 to 2.0, is controlled by

primary microcrack distribution and secondarily by clay infilling, which decreases the range of  $V_p/V_s$ ; (A2), 899 to 907 mbsf with a larger  $V_p/V_s$  range (1.7–2.4), is controlled by primary microcrack distribution without the moderating influence of clay infilling. The velocity range is similar between types (A1) and (A2). Type (b), 725 to 733 mbsf, has no variation in microcracks in the initially deposited material, hence no  $V_p/V_s$  variation, and no opportunity for clay infilling. Macrocracks observed in core are calcite-filled (e.g., Core 104-642E-74) and would account for the small dip in  $V_s$  within the cracked zone as well as the  $V_p/V_s$  range (1.75–2.0).

The basalt flows in this study change in crack porosity from the more massive sections to the brecciated tops of the flows (cf. barrel sheets, Eldholm, Thiede, Taylor et al., 1987). The greater variability in compressional compared with shear velocities over these transitions concurs with the laboratory findings of Stesky (1986). The linear increase in  $V_p/V_s$  with increasing clay content implies that velocity variations are controlled both by microstructure and by subsequent alteration and clay infilling. Infilling of formerly open cracks can serve to stiffen a material, increasing the velocities and decreasing their ratio to counteract the effects of the formerly open microcracks.

## CONCLUSIONS

Depth profiles of the compressional- and shear-wave velocities and  $V_p/V_s$  ratio have been computed, providing reliable Eocene age crustal basement velocity data for the Vøring Plateau escarpment. The compressional interval velocity is 4.14 km/s, shear interval velocity is 2.25 km/s, and  $V_p/V_s$  is 1.84. Compressional and shear velocities correlate well with the companion logs. Within basalt flows  $V_p$  is generally above 5 km/s and  $V_s$  is above 3 km/s. The velocities show a strong sensitivity to lithologic changes and facilitated the discrimination of the flow boundaries.

The similarity in cross plots of density and porosity with and without the clay-rich volcanoclastic layers indicates that changes in physical properties must be due largely to effects other than mineralogy. A careful analysis of the velocity variation over the flows indicates that microstructure in the form of cracks and vesicles could have the primary influence on measured velocities. The alteration to clay is superimposed on this primary structure.

## ACKNOWLEDGMENTS

The authors thank V. G. Goetheus for her assistance with the data analysis, Terrasciences Inc. for their generous gift of Terralog, the log-analysis package used to analyze and display the log data, and F. Paillet for his helpful review.

## REFERENCES

- Archie, G. E., 1942. The electrical resistivity log as an aid in determining some reservoir characteristics. *Tel. Tech.*, 5.
- Brace W. F., Orange, A. S., and Madden, T. R., 1965. The effect of pressure on the electrical resistivity of water-saturated crystalline rocks. *J. Geophys. Res.*, 70:5669–5678.
- Brogliola, C., and Moos, D., 1988. In situ structure and properties of 110 Ma crust from geophysical logs in DSDP Hole 418A. In Salisbury, M. H., Scott, J. H., et al., *Proc. ODP, Sci. Results*, 102: College Station, TX (Ocean Drilling Program), 29–47.
- Cheng, C. H., and Toksöz, M. N., 1980. Modeling of full wave acoustic logs. *Trans. SPWLA, Annu. Logging Symp.*, 21: Paper J.
- Cheng, C. H. and Toksöz, M. N., 1981. Elastic wave propagation in a fluid-filled borehole and synthetic acoustic logs. *Geophysics*, 46: 1042–1053.
- Deer, Howie, and Zussmann, 1966. *An Introduction to the Primary Rock-forming Minerals*: New York (John Wiley and Sons).
- Eldholm, O., Thiede, J., Taylor, E., et al., 1987. *Proc. ODP, Init. Repts.*, 104: College Station, TX (Ocean Drilling Program).

Goldberg, D. S., Gant, W. T., Seigfried, R. W., and Castagna, J. P., 1984. Processing and interpretation of sonic waveforms: a case study. *Trans. SEG 54th Ann. Symp.*, 28-31.

Kimball, C. V., and Marzetta, T. L., 1984. Semblance processing of acoustic array data. *Geophysics*, 49:274-281.

King, M. S., Stauffer, M. R., and Pandit, B. I., 1978. Quality of rock masses by acoustic borehole logging. *Proc. III Int. Congr. I.A.E.G.*, Sec. IV, 1: 156-164.

Moos, D., 1988. Elastic properties of 110 Ma oceanic crust from sonic full waveforms at DSDP Hole 418A. In Salisbury, M. H., Scott, J. H., et al., *Proc. ODP, Sci. Results*, 102: College Station, TX (Ocean Drilling Program), 49-62.

Moos, D., Goldberg, D., Hobart, M. A., and Anderson, R. N., 1986. Elastic wave velocities in layer 2A from full waveform sonic logs at Hole 504B. In Leinen, M., Rea, D. K., et al., *Init. Reports DSDP*, 92: Washington (U.S. Govt. Printing Office), 563-570.

Moos, D., and Zoback, M. D., 1983. In-situ studies of velocity in fractured crystalline rock. *J. Geophys. Res.*, 88: 2345-2358.

Nur, A., 1980. *Wave Propagation in Porous Rocks*: Stanford, CA (Stanford University Rock Physics Project), Vol. 13.

Paillet, F. L., and White, J. E., 1982. Acoustic modes of propagation in the borehole and their relationship to rock properties. *Geophysics*, 47: 1215-1228.

Schlumberger, 1972a. *Log Interpretation. Volume 1, Principles*: New York (Schlumberger Ltd.).

Schlumberger, 1972b. *The Essentials of Log Interpretation Practice. Service Techniques*: France (Schlumberger).

Serra, O., 1984. *The Fundamentals of Log Interpretation*: Amsterdam (Elsevier).

Shipboard Scientific Party, 1987. Site 642: Norwegian Sea. In Eldholm, O., Thiede, J., Taylor, E., et al., *Proc. ODP, Init. Repts.*, 104: College Station, TX (Ocean Drilling Program), 53-453.

Stephanson, O., Lande, G., and Bodare, A., 1979. A seismic study of shallow jointed rock. *Int. J. Rock Mech. Min. Sci. Geomech. Abst.*, 16: 319-327.

Stesky, R. M., 1986. Compressional and shear velocities of dry and saturated jointed rock: A laboratory study. *Geophys. J. R. Astron. Soc.*, 83: 239-250.

Stierman, D. J., and Kovach, R. L., 1979. Pressure induced velocity gradient: an alternative to a Pg refractor in the Gabilan Range, central California. *Bull. Seis. Soc. Am.*, 69: 397-415.

Swolfs, H. S., Brechtel, C. E., Brace, W. F., and Pratt, H. R., 1981. Field mechanical properties of a jointed sandstone. In Carter, N. L., Friedman, M., Logan, J. M. (Eds.), *Mechanical Behavior of Crustal Rocks (the Handin Volume)*. *Geophys. Monogr.*, 24: Washington (Am. Geophys. Union), 161-172.

Timoshenko, S. P., and Goodier, J. N., 1934. *Theory of Elasticity*: New York (McGraw-Hill).

Tsang, L., and Rader, D., 1979. Numerical evaluation of the transient acoustic waveform due to a point source in a fluid-filled borehole. *Geophysics*, 44: 1706-1720.

Turuta, N. U., Galimullin, A. T., Blagodarenko, Y. U., Panchenko, D. F., Karpinskii, A. V., and Ruzin, V. I., 1967. Velocity of propagation of elastic waves in a fissured medium. *Soviet Min. Sci.*, 1: 27-31.

Von Herzen, R. P., Francis, T.J.G., and Becker, K., 1983. *In situ* large scale electrical resistivity of ocean crust, Hole 504B. In Cann, J. R., Langseth, M. G., Honnorez, J., Von Herzen, R. P., White, S. M., et al., *Init. Repts. DSDP*, 69: Washington (U.S. Govt. Printing Office), 237-244.

Willis, M. E., and Toksöz, M. N., 1983. P and S velocity determination. *Annual Report of the M.I.T. Full Waveform Acoustic Logging Consortium*, Sec. 7.

Date of initial receipt: 15 April 1987  
 Date of acceptance: 14 April 1988  
 Ms 104B-147

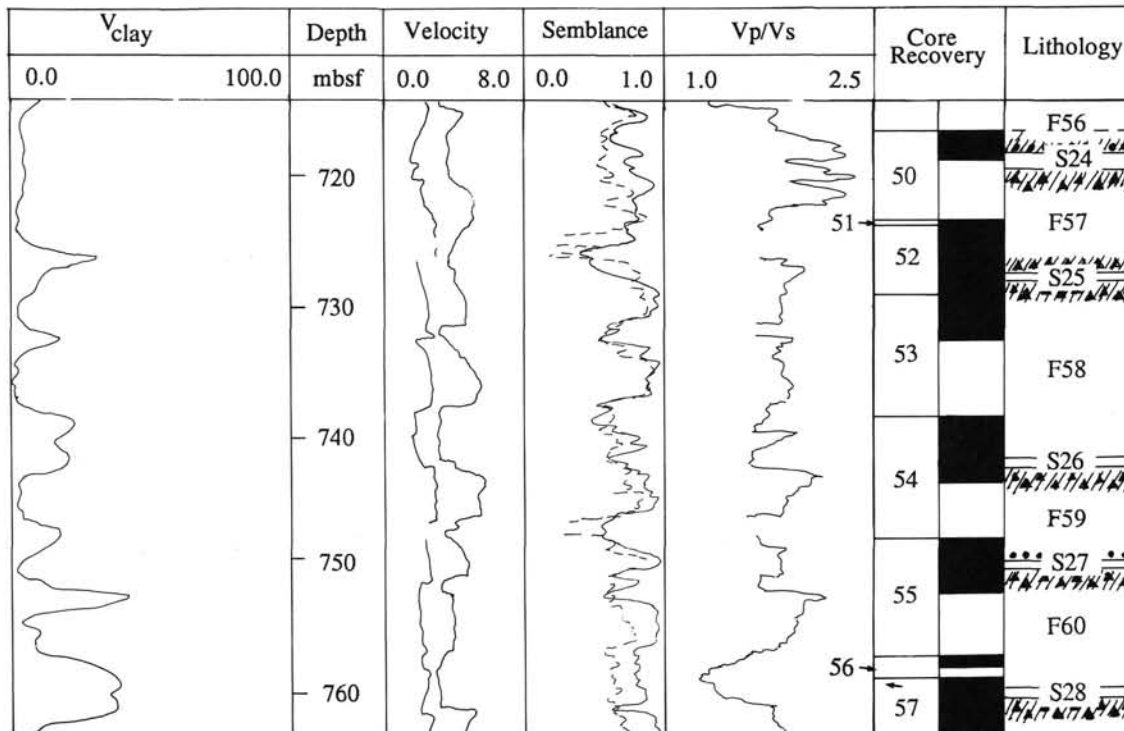


Figure 10. Detailed plot of the velocity logs and clay content measured within the interval 711 to 761 mbsf correlated with the corresponding section of the lithostratigraphic column determined from petrographic analysis. This interval corresponds to a series of seven of the Group II fine-grained type flows of the upper series.

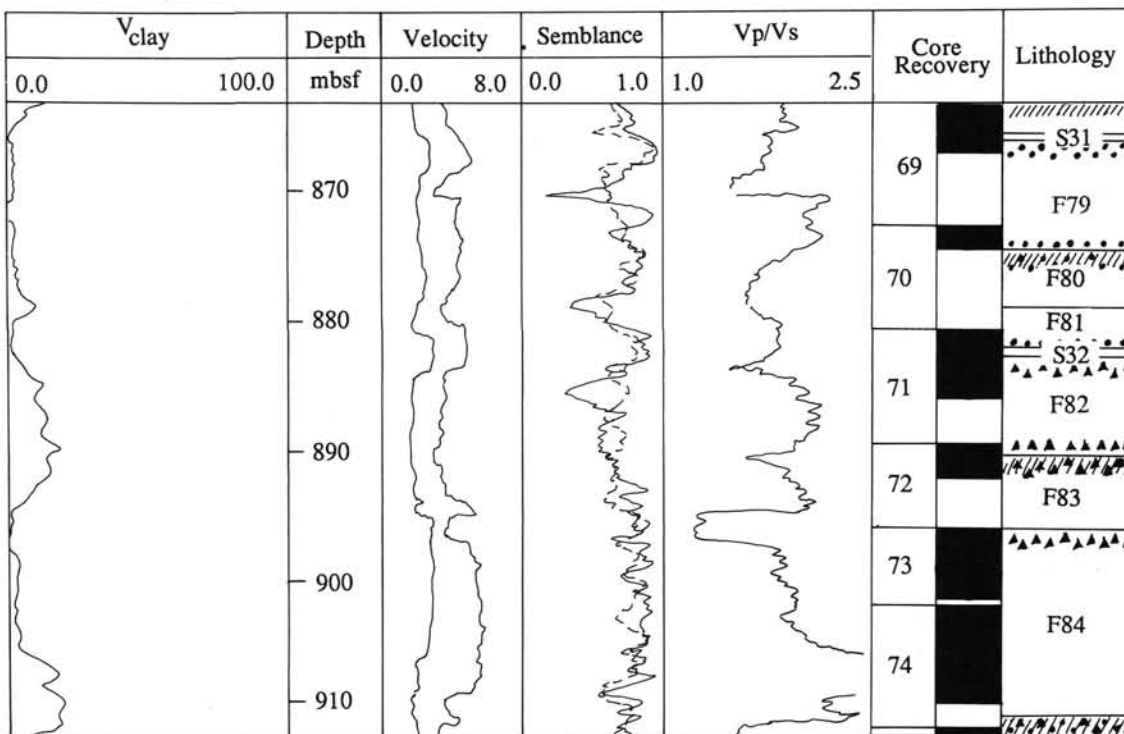


Figure 11. Detailed plot of the velocity logs and clay content measured within the interval 861 to 911 mbsf, correlated with the corresponding section of the lithostratigraphic column where there is a transition at 879 mbsf from Group II to Group III flow types. The intervals 873 to 879 mbsf and 896 to 907 mbsf represent a flow type that does not show a gradual increase in velocity with depth.

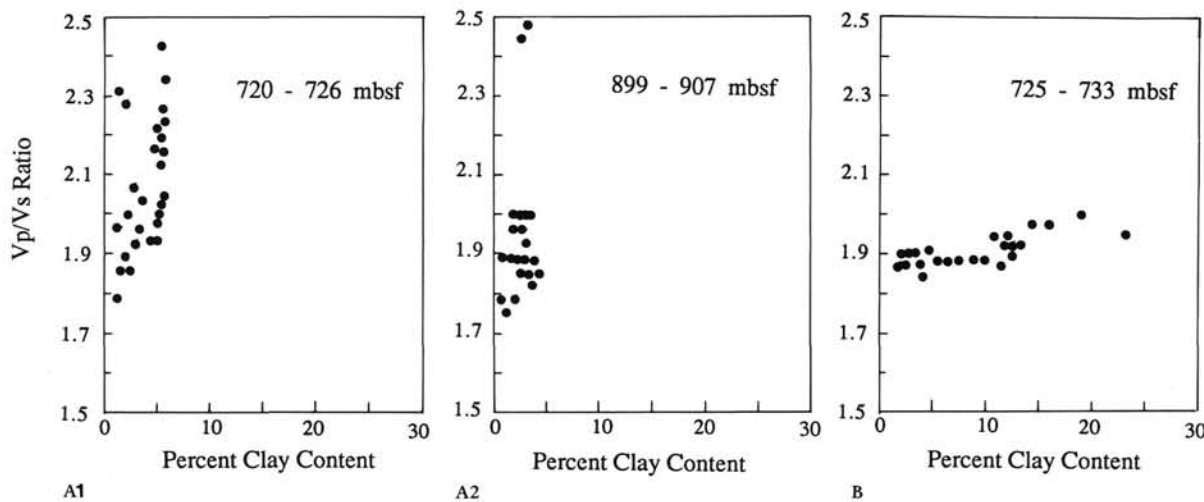


Figure 12. The two primary types of flows found from this velocity analysis can be distinguished by the variation in velocity with depth: (A) sharply increasing  $V_p$  and (B) constant  $V_p$ . Type (A) has decreasing  $V_p/V_s$  with increasing depth. Sometimes clay content also decreases (A1); in other cases clay content is uniformly low (A2).